Laser Physics, Vol. 4, No. 5, 1994, pp. 1066 - 1075.

SPECIAL ISSUE
"LASER COOLING AND TRAPPING"

Trap Loss Collisions of ^{7}Li: The Role of Trap Depth

N. W. M. Ritchie, E. R. I. Abraham, and R. G. Hulet

Physics Department and Rice Quantum Institute, Rice University, Houston, Texas 77251, USA

Received June 2, 1994

Abstract – We present experimental measurements of the rate of loss of ultracold ^{7}Li from a magnetooptical trap (MOT) produced by collisions between the trapped atoms. The loss rate was measured for a range of trap laser intensities and detunings. Since fine-structure changing collisions may be suppressed as a loss mechanism in Li, it is possible to isolate the loss due to that mechanism from the radiative escape mechanism. The measured rates are compared with recent theoretical calculations. Relatively good agreement is found for the magnitude of the loss rate, but there is disagreement as to the qualitative dependence on trap laser detuning and intensity. In many respects, Li is ideal for comparisons of trap loss measurements with theory, since the interatomic potentials for Li are relatively well known. We also present a realistic calculation of trap depth, or equivalently, escape velocity. This fully three-dimensional calculation incorporates all relevant atomic levels. We demonstrate that accurate knowledge of the trap depth is essential for quantitative comparisons of experimental loss rate measurements with theory.

1. INTRODUCTION

Laser-cooling techniques are capable of producing samples of atoms at temperatures and densities that were previously unattainable. At ultralow temperatures ($\ll$1 K), collisions between atoms exhibit unique and interesting features. Unlike collisions at higher temperatures, ultracold collisions are significantly influenced by the long-range part of the interaction potential. For collisions involving excited states, such as those occurring in magnetooptical atom traps, the collision duration can be comparable to the excited-state radiative lifetime. Therefore, photoexcitation/deexcitation processes are important. Investigations of collisions that cause atoms to be ejected from the trap provide insight into radiative processes of atoms interacting at long range and enhance our understanding of effects that fundamentally limit the attainment of higher trapped atom densities.

Two exoergic two-body collision mechanisms, radiative escape (RE) and fine-structure changing collisions (FS), have been identified to explain the loss of trapped alkali atoms from a magnetooptical trap (MOT) [1]. In both cases, an atom pair, both in the atomic $S_{1/2}$ ground state and in close proximity (~1000 Å), absorb a near-resonant trap laser photon. They may interact via the attractive R^{-3} resonant dipole interaction, causing them to accelerate toward each other. Since the collision duration may be comparable to the radiative lifetime, the atom pair may radiate a photon during the collision, which is less energetic than the trap laser photon by an amount ΔE. If 1/2 ΔE is greater than the trap depth E_T, the atoms gain sufficient energy to escape the trap, producing an RE trap loss event. In the FS mechanism, the atom pair is initially excited to a molecular state correlating with $S_{1/2} + P_{3/2}$ atomic states. At small interatomic separation, the pair makes a Landau–Zener transition to a molecular state correlating with $S_{1/2} + P_{1/2}$ atomic states. The atoms share the fine-structure energy difference, ΔE_{FS}, which leads to escape when $E_T < 1/2\ \Delta E_{FS}$.

For alkali atoms, these trap loss collision processes have been studied for Na [2, 3], Cs [4], Rb [5 - 7], and recently for Li [8, 9]. Li is unique among the alkali atoms in that ΔE_{FS} (0.48 K) is in the range of trap depths readily achievable by a MOT, enabling a separation of loss due to RE from FS [8, 9]. For the case $E_T < 1/2\ \Delta E_{FS}$, variation of the trap depth can be used to study both loss mechanisms, while for $E_T > 1/2\ \Delta E_{FS}$, the FS mechanism is suppressed as a loss mechanism, and radiative escape collisions may be studied. In both regimes, more precise comparison with theory is possible.

Trap depth is, therefore, a critical parameter for understanding trap loss. It is an oversimplification, however, to describe the trap depth by a single value E_T, since the depth of an optical trap is likely to be different for atomic motion along different directions, relative to the trap laser beams. Efforts have been made to calculate trap depth, or equivalently, escape velocity [10], but directional dependence has not been properly accounted for. In this paper, a three-dimensional model that includes all relevant atomic levels is presented. The model is applied to recent observations of trap loss for ^{7}Li in a four-beam tetrahedral MOT [8] and in a six-beam MOT [9]. The measured loss rate coefficients are compared with a semiclassical theory [11], in which trap depth is taken into account. Accurate measurements of trap loss rates for Li are important because accurate comparisons with theory are facilitated by relatively well-known Li_2 molecular potentials, which are reliably determined by *ab initio* calculation [12].

2. TRAP DEPTH MODEL

A MOT consists of four or more near-resonant laser beams that provide for dissipation of the atomic kinetic energy and, when combined with an inhomogeneous magnetic field, produce a restoring force in the three orthogonal directions [13]. In our trap depth model, the classical equations of motion for an atom in the combined laser and magnetic fields of the trap are integrated to determine its trajectory in the three spatial dimensions. The trap depth is defined by $E_T = 1/2\, m v_e^2$, where v_e is the maximum velocity that may be imparted to an atom initially at trap center for it to remain trapped. It should be emphasized that the trap depth is determined by dissipative rather than conservative forces in a MOT. This same model can be used to calculate the capture velocity of a MOT [10].

The force on an atom, $\mathbf{F}(\mathbf{x}, \mathbf{v})$ (quantities in bold typeface are three-dimensional vectors), at a time t, position $\mathbf{x}(t)$, and velocity $\mathbf{v}(t)$ is calculated by summing the individual contributions to the force produced by each trap laser beam. Only Doppler cooling forces [14] are considered, while stimulated or dipole forces and forces arising from multiphoton excitation are neglected. Also neglected are polarization gradient forces since they are small for velocities as large as v_e. The force contributed by the ith laser beam is

$$\mathbf{F}_i = \hbar \mathbf{k}_i \sum_{n', n} R_i(n', n)\, (\rho_{n'} - \rho_n)\,, \tag{1}$$

where $\mathbf{k}_i$ is the wave vector of the ith laser beam; n' and n refer to ground-state and excited-state sublevels, respectively; and $R_i(n', n)$ is the stimulated rate from level n' to level n, due to the ith laser beam. For a given $\mathbf{x}$, the populations ρ_n, where n refers here to any atomic level, are calculated in steady state, for which

$$\begin{aligned} 0 = \sum_{n'} [&- \rho_n R(n, n') - \rho_n A(n, n')\Gamma \\ &+ \rho_{n'} R(n', n) + \rho_{n'} A(n', n)\Gamma\ ]\,. \end{aligned} \tag{2}$$

The sum extends over all atomic levels. The total stimulated rate from level n' to level n due to all laser beams is $R(n', n) = \sum_i R_i(n', n)$. $A(n, n')$ is the branching ratio for spontaneous decay from level n to level n', which is equal to zero when n is a ground level and Γ is the spontaneous decay rate of the excited state. The ρ_n are normalized such that $\sum_n \rho_n = 1$.

The basis states are chosen to be eigenstates of a Hamiltonian H that consists of terms representing the unperturbed atom, including hyperfine interactions, and the interaction of the atomic magnetic dipole moment with the local magnetic field $\mathbf{B}(\mathbf{x})$. Both the direction and magnitude of $\mathbf{B}(\mathbf{x})$ vary with position. The field is calculated using the fifth-order series expansion of the magnetic field produced by two current loops in the anti-Helmholtz configuration [15]. In zero magnetic field, the energy eigenstates are $|\xi, J, I, F, m_F\rangle$, where ξ is the principal quantum number, J is the total electronic angular momentum, I is the nuclear spin, F is the total angular momentum, and m_F is the projection of F onto the quantization axis determined by the local direction of $\mathbf{B}(\mathbf{x})$. Diagonalizing H yields the eigenvalues, $E_n(\mathbf{B})$, and the eigenstates expressed as a superposition of the zero-field states:

$$|n;\mathbf{B}\rangle = \sum_{F, m_F} \alpha_n(J, F, m_F;\mathbf{B})\, |J, F, m_F\rangle. \tag{3}$$

For simplicity, the labels ξ and I have been omitted. For ^{7}Li, $I = 3/2$, so there are eight $2S_{1/2}$ ground-state levels, and sixteen $2P_{3/2}$ excited-state levels in the Hamiltonian matrix. The trap laser frequencies are assumed here to be near resonant with the $S_{1/2} \longleftrightarrow P_{3/2}$ transition, although other transitions may be considered by simple modification.

Each laser beam and laser frequency component is denoted by the subscript i. A beam is defined by its wave vector $\mathbf{k}_i$, intensity I_i, frequency ω_i, and polarization $\vec{\sigma}_q$. The stimulated rate between two eigenstates of H due to the ith beam is [16]

$$\begin{aligned} R_i(n, n';x) = 6\pi \lambda\!\!\!^{-2} \frac{I_i(\boldsymbol{x})}{\hbar\, \omega_i} &\left(\frac{(\Gamma/2)^2}{(\Gamma/2)^2 + \delta_i(n, n';\boldsymbol{v}, \mathbf{B})^2} \right) \\ &\times \left| \sum_{\substack{F, m_F \\ F', m_{F'} \\ q}} \left(\alpha_{n'}(F', m_{F'};\ \mathbf{B})^* \alpha_n(F, m_F;\mathbf{B}) \right.\right. \\ &\times \varepsilon_i(q)\, (-1)^{(F' - m_{F'} + F)} \sqrt{(2F+1)\,(2F'+1)\,(2J'+1)} \\ &\left.\left. \times \{ \begin{matrix} J' & F' & I \\ F & J & 1 \end{matrix} \} \begin{pmatrix} F' & 1 & F \\ -m_{F'} & q & m_F \end{pmatrix} \right) \right|^2, \end{aligned} \tag{4}$$

where $q = +1$, 0, and -1, and $\vec{\sigma}_q$ signifies one of the polarization basis states $\vec{\sigma}_+$, $\vec{\pi}$, and $\vec{\sigma}_-$ along the quantization axis defined by the direction of $\mathbf{B}(\mathbf{x})$. The projection of the laser polarization onto a basis state $\vec{\sigma}_q$ is $\varepsilon_i(q) = \vec{\sigma}_i \cdot \vec{\sigma}_q$. The curly brackets signify a 6-j symbol, the following brackets signify a 3-j symbol, $\lambda\!\!\!^{-}$ is the wavelength of the transition divided by 2π, and the detuning from resonance is $\delta_i(n, n';\boldsymbol{v}, \mathbf{B}) = \omega_i - \mathbf{k}_i\boldsymbol{v} - |E_{n'} - E_n|/\hbar$. R_i depends on position via the spatial dependence of the intensity distribution of the laser beam $I_i(\mathbf{x})$ and via $\mathbf{B}(\mathbf{x})$.

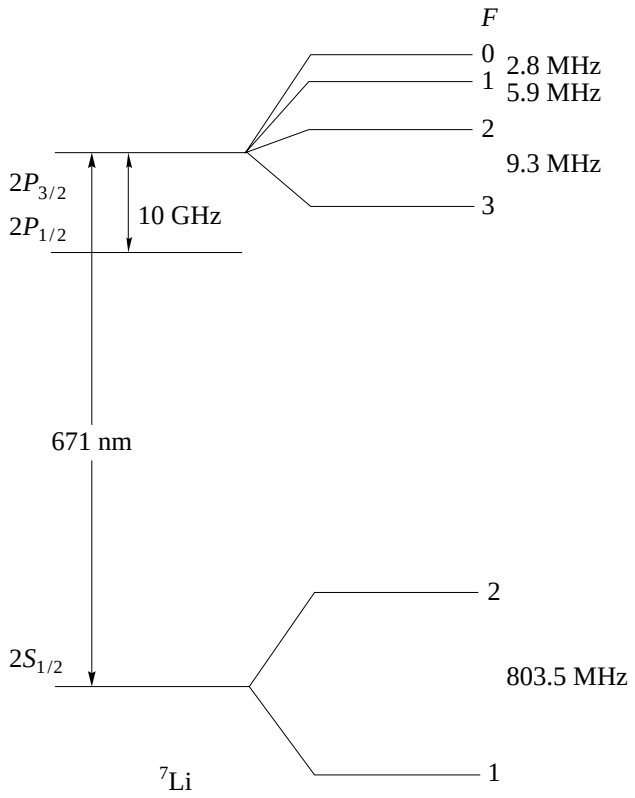

Fig. 1. Energy levels of the $2S_{1/2}$ ground state and the $2P_{1/2}$ and $2P_{3/2}$ excited states of ^{7}Li.

3. EXPERIMENT

The six MOT laser beams are derived from a dye laser that is frequency locked relative to a saturated absorption feature of Li vapor in a heat pipe cell to provide a relative frequency reference and long-term frequency stability. Both the $2S_{1/2}$, $F = 1 \longleftrightarrow 2P_{3/2}$, $F = 2$ and $2S_{1/2}$, $F = 2 \longleftrightarrow 2P_{3/2}$, $F = 3$ transitions (Fig. 1) are driven with equal intensity. The two frequency components are the first-order sidebands obtained by frequency modulating the laser beams at 406.4 MHz with an electro-optical modulator. The detuning Δ of the lower sideband from the $2S_{1/2}$, $F = 2 \longleftrightarrow 2P_{3/2}$, $F = 3$ resonance frequency equals the detuning of the upper sideband from the $2S_{1/2}$, $F = 1 \longleftrightarrow 2P_{3/2}$, $F = 2$ resonance frequency. To create a near spherically symmetric cloud of trapped atoms, the intensity of the four radial beams are made equal while the intensity of an axial beam is set at 60% the intensity of a radial beam. The beam waist ($1/e^2$ intensity radius) of each beam is 0.64 cm, and the beams are apertured to a radius of 0.71 cm. A pair of anti-Helmholtz configured coils generates a magnetic field gradient of 30 G/cm in the axial direction and 15 G/cm in the radial direction. The trap is loaded from a chirp-slowed atomic beam [17]. The frequency chirp is generated using a broadband traveling-wave electro-optic modulator. The chirp-slowing beam may be chopped off using an acousto-optic modulator to cease trap loading.

A measurement of the trap loss rate is accomplished by loading the trap, chopping off the chirp-slowing beam, and then observing the decay in the trap fluorescence, similar to the procedure described by Prentiss *et al.* [2]. Two mechanisms contribute to loss of trapped atoms: collisions with hot background gas atoms and collisions among trapped atoms [1]. The rate of change of the number of trapped atoms N is given by

$$\frac{dN}{dt} = -\gamma N - \beta \int\limits_{\text{all space}} n^2 d^3x, \tag{5}$$

where n is the density distribution of trapped atoms, γ is the rate of loss from background gas collisions, and β is the rate of two-body trap loss collisions.

The number of excited-state atoms in the cloud of trapped atoms is measured by detecting their trap laser-induced fluorescence with a calibrated silicon photodiode. The number of ground-state atoms can then be calculated using (2) for the steady-state populations. The density distribution is found by imaging the cloud with a CCD video camera. For all trap conditions, the cloud is observed to be Gaussian in shape. However, the size of the cloud size grows with increasing N, presumably because of the increased optical thickness of the cloud and the reabsorption of fluorescence [18, 19]. Empirically, the Gaussian parameters vary with N as

$$w_i(N(t)) = a_i + b_i \frac{N(t)}{N_o}, \tag{6}$$

where i refers either to the axial (A) or radial (R) dimension and N_o is the initial number of atoms. The parameters a_i and b_i are measured for each combination of trap laser detuning Δ and intensity I. With these assumptions, the integral in (5) reduces to $N^2/((2\pi)^{3/2} w_A(N) w_R(N)^2)$. Depending on Δ and I, the maximum density n_o ranges between 2×10^9 cm^{-3} and 5×10^{10} cm^{-3}, and w_R and w_A are initially between 100 μm and 900 μm. For most of the Δ, I combinations, $w_R \approx w_A$ to within 20% for all N. In most cases, $b_i/a_i < 0.5$, and in all cases, $b_i/a_i < 0.8$.

Our observation that the trapped atom cloud remains Gaussian in shape at the highest densities observed is contrary to previous investigations [19, 20]. In those investigations, the central density was observed to be uniform at the highest densities due to effects caused by the optical thickness of the trapped atom cloud. Our maximum density of 5×10^{10} cm^{-3} is comparable to the maximum observed by other groups. Apparently, the differences must be ascribed to differences in the trapping characteristics of lithium compared with the other alkali species or to differences in our experimental setup. Unlike the other experiments, we made no effort to shield the Earth's magnetic field, which likely inhibits sub-Doppler cooling mechanisms. The restoring force produced by the usual Doppler radiative force is weaker than that provided by sub-Doppler mechanisms [20], leading to a larger trap that

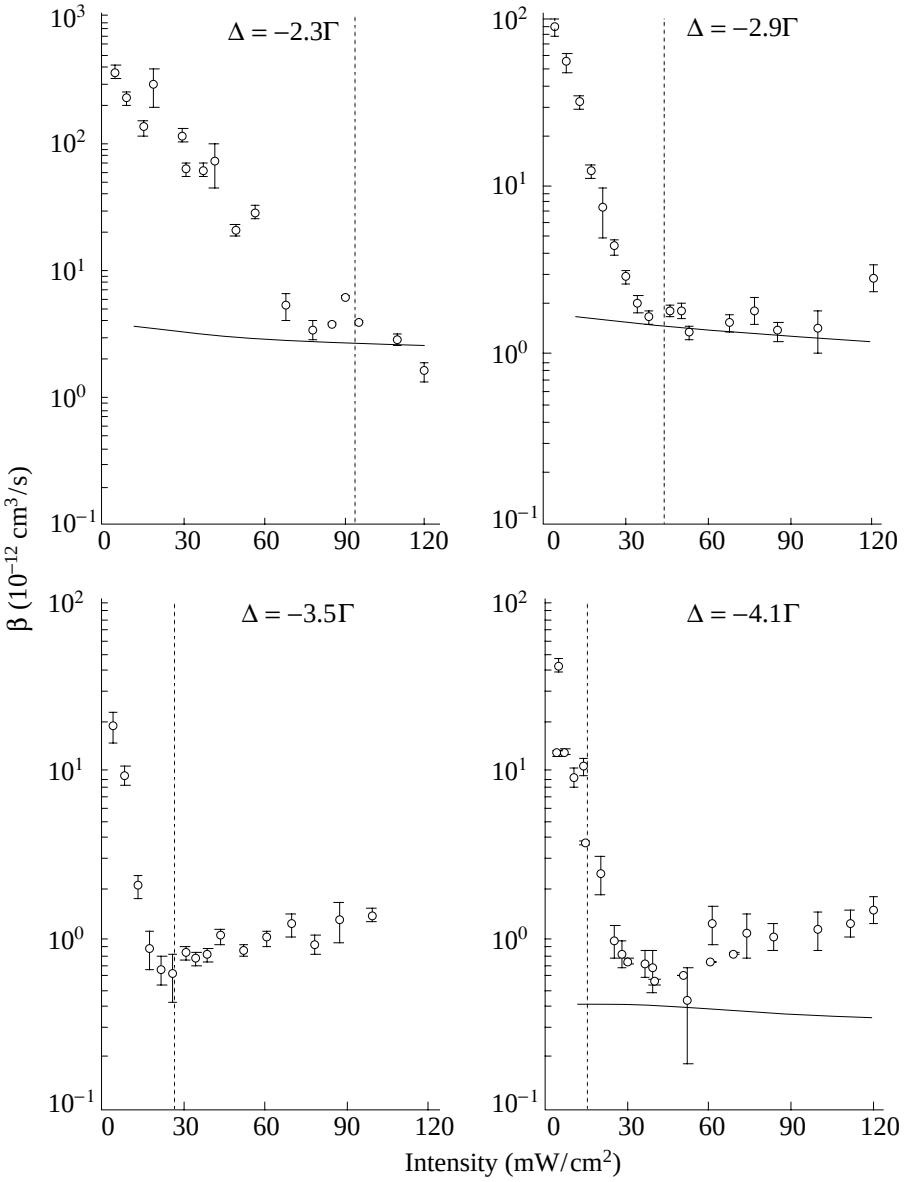

Fig. 2. Data corresponding to two-body trap loss collisions as a function of trap laser intensity for several trap laser detunings. The open circles correspond to the average of ten, or in several cases, five trap decay measurements. The error bars signify the one standard deviation range for the multiple measurements. The dotted vertical line on each plot indicates the intensity for which the trap depth model predicts fine-structure changing collisions no longer lead to losses from the trap. At higher intensities, only RE collisions contribute to the total loss rate. The solid line is the result of a semiclassical, optical Bloch equation calculation of the RE collisional loss rate provided by Julienne *et al*. [11] and averaged over the anisotropic trap depth using the trap depth model.

requires more atoms to achieve the limiting density. Second, our experiment was performed using trap laser detunings and intensities that are generally higher than those of other experiments. In our case, the fractional absorption of the trap laser beam intensity is less, thereby reducing the importance of optical thickness. Kawanaka *et al.* [8] do observe a non-Gaussian density distribution in a Li tetrahedral MOT, but only for trapped atom cloud diameters exceeding 4 mm [21], much larger than our cloud sizes.

The population calculations were checked by measuring the total trapped atom density using optical absorption [2, 22]. In this measurement, a weak (~500 nW/cm^2) probe laser beam with a Gaussian beam waist ($1/e^2$ intensity radius) of ~100 μm is passed through the center of the trap. The frequency of the probe is scanned through the $2S_{1/2} \leftrightarrow 2P_{1/2}$ and $2S_{1/2} \leftrightarrow 2P_{3/2}$ resonance frequencies while the absorption of the beam is measured. To ensure that all atoms are in the ground state, the trap beams are gated off every 500 μs for a duration of 50 μs; the absorption is measured during the off period. The fraction of the probe beam that is transmitted is $e^{-\sigma\int n\,dl}$, where the integration is over the path of the probe beam and σ is the

excitation cross section. The beam waist of the probe beam is accounted for in this calculation. The spatial dimensions of the trapped atom cloud found using the CCD camera combined with absorption measurements yield the density distribution n and N_0. The absorption measurement provides a measurement of the density to within an estimated uncertainty of a factor of two. Combining the measurement of total trap fluorescence with N_0 yields the excited-state fraction. This procedure for measuring the excited-state fraction was compared with the calculated values from equation (2) for several combinations of trap parameters. Agreement was found to be within the measurement uncertainty. We believe that the calculation provides more precise values for the excited-state fraction than does the absorption measurement, so the calculated values are used to extract the loss rate coefficient from the data.

The high-resolution trapped atom absorption spectrum can also be used to verify the frequency detuning Δ of the trap laser locked to the Li vapor heat pipe. This is accomplished by heterodyning a portion of both a trap laser beam and the absorption probe tuned to the $2S_{1/2}$, $F = 2 \longleftrightarrow 2P_{3/2}$, $F = 3$ feature on a fast silicon photodiode and measuring the relative frequency difference. Frequency variations of the lasers produce a relative uncertainty between the various values of Δ of ± 1 MHz, while the estimated absolute uncertainty in Δ is ± 2 MHz.

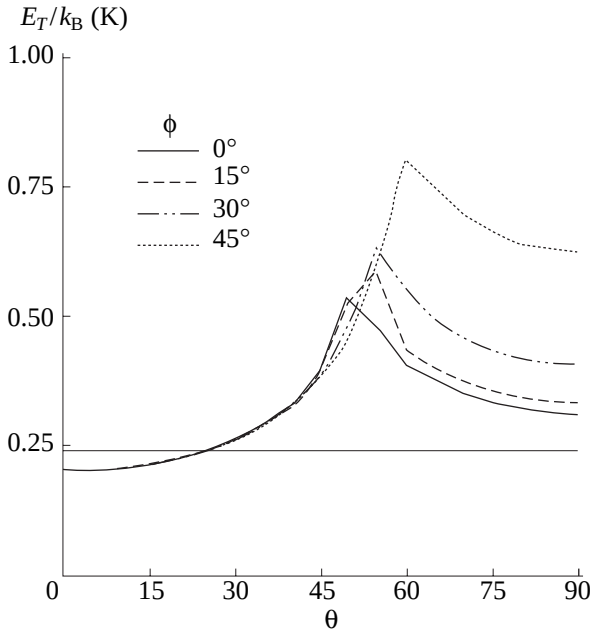

Fig. 3. Angular variation of trap depth for a six-beam MOT with detuning of -2.3Γ and intensity of 48 mW/cm^2. The other trap parameters are those of the actual trap used in the experiment and described in the text. The horizontal axis is the polar angle, θ. E_T is shown for four azimuthal angles ϕ contained in one-half of an octant of a sphere, which, through symmetry, is sufficient to define E_T for the entire sphere. The solid line at $1/2\,\Delta E_{FS}/k_B = 0.24$ K separates the region for which FS leads to trap loss from the region in which FS is suppressed as a loss mechanism.

Figure 2 shows data for four values of Δ and a range of I, the total intensity in each of the two sideband frequencies. The measured values of β are shown as open circles. These represent the average of 10 data runs (or five, in several cases), where β is found from each fluorescence decay curve by fitting equation (5). The error bars represent one standard deviation from the mean for the 10 data runs. The run-to-run variation is primarily caused by fluctuations of the laser frequency of ~0.5 MHz with a time constant of 1 - 2 s. The effect of frequency fluctuations of this time scale can be minimized by lengthening the trap decay time γ^{-1}, which is determined by the rate of collisions with background gas atoms. Most of the measurements were made with a vacuum pressure of $\sim 10^{-9}$ Torr, for which $\gamma^{-1} = 5$ - 20 s, depending on trap parameters. Some points at $\Delta = -4.1\Gamma$ were taken with a pressure of 10^{-10} Torr, for which $\gamma^{-1} \approx 100$ s. We found that aperturing the atomic beam to block line-of-sight from the atomic beam oven nozzle to the trapped atom cloud lengthens decay time. For the same reason, the beam is operated at a relatively low temperature (450 - 500°C) to reduce the beam flux. Since thermal Li is observed to have a large bounce probability on stainless steel and glass, the window in direct line-of-sight of the beam was moved ~1 m downstream of the trap. We estimate that our uncertainty in β from systematic effects, primarily the measurement of the trapped atom cloud size, is 50%.

Previously, we tried to measure trap loss rates in a MOT loaded directly from the vapor of a cell [23]. Although Li can be successfully loaded into the trap by operating the cell at ~200°C, two-body trap loss was unobservable because of the large rate of background gas collisions.

4. DISCUSSION

Figure 3 displays calculated values of $E_T(\theta, \phi)$ for a six-beam MOT with $I = 48$ mW/cm^2 and $\Delta = -2.3\Gamma$ ($\Gamma = 2\pi \times 5.8$ MHz) as a function of polar angle θ and azimuthal angle ϕ in one-half of one octant. The six trap beams propagate along $(\theta, \phi) = (0, 0), (180°, 0°), (90°, 0°), (90°, 90°), (90°, 180°)$, and $(90°, 270°)$. In this half octant, E_T varies from less than $1/2\ \Delta E_{FS}$ ($= 0.24$ K) along the axial direction, (0, 0), to greater than 0.8 K along (62°, 45°). Several factors contribute to make the axial direction the shallowest. First, the intensity of an axial beam is only 60% of that of a radial beam. The trap is operated with unequal beam intensities to ensure near-spherical symmetry of the trap size. Second, and most important, for an atom moving sufficiently fast, the velocity-dependent detuning $\Delta - \mathbf{k}\cdot\mathbf{v}$ can be minimized for an atom moving along a diagonal axis rather than collinear with a trap beam axis. For an atom moving in a beam direction, for example, a laser detuning of -2.3Γ is compensated by the Doppler shift for $v \approx 9$ m/s, a velocity that is considerably below the escape velocity

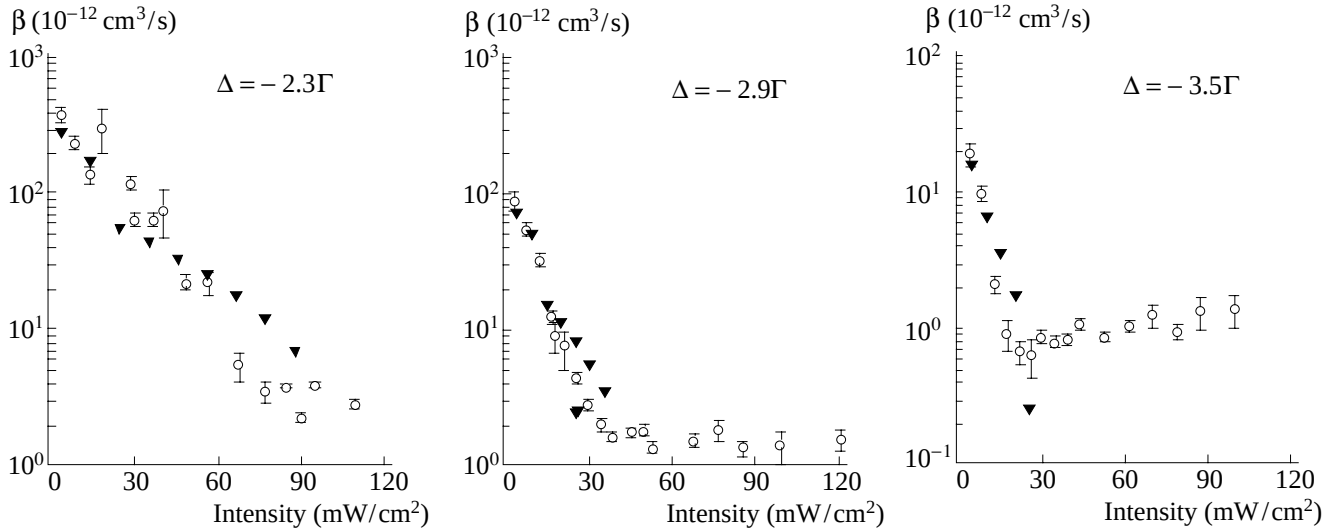

Fig. 4. Extraction of the total fine-structure changing rate coefficient B_{FS}, independent of whether it leads to loss, for detunings Δ of -2.3Γ, -2.9Γ, and -3.5Γ. The open circles represent the same data presented in Fig. 2. The triangles are the result of fitting the data to equation (7). The measured loss rates, β_{FS}, decrease with I as the fraction of the trap solid angle shallow enough to permit atoms undergoing FS collisions to escape, diminishes. The rate coefficient B_{FS} is found to be 3×10^{-10} cm^3/s, 1×10^{-10} cm^3/s, and 5×10^{-11} cm^3/s, respectively, for the three detunings, independent of intensity.

at $\Delta = -2.3\Gamma$, for the entire range of I investigated. Therefore, the maximum force should occur in directions minimizing the Doppler shift, such as in the (55°, 45°) direction. The slight deviation from this prediction evident in Fig. 4 is due to the smaller intensity and greater magnetic field gradient in the axial direction. We find that a larger field gradient results in a smaller trap depth, for our range of parameters, since the field increases the effective detuning further to the blue.

Data for each of the four detunings represented in Fig. 2 show that the measured loss rate is largest at small intensities and initially decreases with increasing I until reaching a distinct minimum, which occurs at a different value of I for each detuning. We attribute this loss rate minimum to the suppression of FS as a loss mechanism, which occurs when $E_T > 1/2\ \Delta E_{FS}$ [9], as was also recently observed for ^{7}Li by Kawanaka *et al.* [8]. At higher values of I, the loss is due entirely to RE. In the RE regime, the loss rate is significantly smaller than at lower intensities, where FS dominates. The dashed vertical lines in Fig. 2 indicate the intensity where $E_T \geq 1/2\ \Delta E_{FS}$ for all trajectory angles. At higher intensities, FS is suppressed as a loss mechanism. A similar suppression of ground-state hyperfine changing collisions as a loss mechanism was observed by Sesko *et al.* [4] and by Wallace *et al.* [6] in the case of Cs and Rb, respectively.

For the parameters of Fig. 3, $E_T < 1/2\ \Delta E_{FS}$ for some fraction of the trap solid angle. These directions are shallow enough to permit fine-structure changing collision products to escape. For E_T greater than the horizontal line shown in Fig. 3, FS is suppressed as a loss mechanism. Thus, if the total rate of fine-structure changing collisions, regardless of whether they produce loss, is $B_{FS}(\Delta, I)$, the corresponding measured loss rate is

$$\beta_{FS}(\Delta, I) = \frac{B_{FS}(\Delta, I)}{4\pi} \int_{4\pi} \Phi(\Delta E_{FS} - E_T(\theta, \phi)) d\Omega, \quad (7)$$

where $\Phi(x)$ is 1 when $x > 0$ and 0 when $x < 0$. Equation (7) predicts that β_{FS} decreases as a greater fraction of the solid angle of the trap is closed to FS loss, as is observed. Equation (7) combined with calculations of $E_T(\theta, \phi)$ may be used to fit the data of Fig. 2 in order to extract B_{FS}. B_{FS} is the fine-structure changing collision rate, independent of trap depth, and is the quantity most naturally compared with theory. In Fig. 4, the data are replotted along with the results of such a fit for the smallest three detunings. For each Δ, the best fit assumes a constant B_{FS}, independent of I. We find $B_{FS} = 3 \times 10^{-10}$ cm^3/s for $\Delta = -2.3\Gamma$, $B_{FS} = 1 \times 10^{-10}$ cm^3/s for $\Delta = -2.9\Gamma$, and $B_{FS} = 5 \times 10^{-11}$ cm^3/s for $\Delta = -3.5\Gamma$. The fits agree qualitatively with the data for all three values of Δ.

The observed I and Δ dependence of B_{FS} are at odds with the semiclassical theory of Julienne, Williams, Dulieu, and Band (JWDB), although there is agreement as to the order of magnitude [11]. In the absence of trap depth effects, JWDB predict that B_{FS} increases with increasing I, as the product of the excited-state fraction ρ_e and the ground-state fraction $1 - \rho_e$ increases. We attempted to fit the data with a B_{FS} that increases as $\rho_e(1 - \rho_e)$, where ρ_e is calculated using equation (2). The resulting loss rate coefficients β_{FS} drop less steeply with I than do the data of Fig. 4. We note that ρ_e calculated using equation (2) with all

24 relevant hyperfine levels agrees quite well with the excited-state population of a two-level system, $\rho_e^{(2)}$,

$$\rho_e^{(2)} = \frac{I/I_s}{2I/I_s + 4\Delta^2 + \Gamma^2}, \quad (8)$$

with saturation intensity $I_s = 7.6$ mW/cm^2. The value $I_s = 7.6$ mW/cm^2 corresponds to a resonant excitation cross section of $4\pi\lambda^2$ and gives a saturation curve for B_{FS} that is consistent with JWDB, Fig. 6 [11], for their optical Bloch equation theory [24]. JWDB find that the total rate of FS for Li is the sum of contributions from the long-range, Hund's case (c) 0_u^+ and 2_u molecular states. They show that the intensity dependence for excitation of each of the two molecular states is quite different. From their Fig. 11, we conclude that $I_s \approx 3$ mW/cm^2 for the 0_u^+ state and $I_s > 100$ mW/cm^2 for the 2_u state, because transitions from 2_u to the ground state are forbidden in the electric dipole approximation. Therefore, we attempted to fit the data assuming the intensity dependence of the excitation is that of the 0_u^+ state, that is, with $\rho_e^{(2)}$ evaluated with $I_s = 3$ mW/cm^2. Again, the fit does not fall as steeply with I as do the data. As expected, accounting for the $\rho_e(1-\rho_e)$ factor causes the fitted loss rate coefficient, β_{FS}, to reach a maximum at low intensity, at $I = 9$ mW/cm^2 for $\Delta = -2.3\Gamma$, and at $I = 12$ mW/cm^2 for $\Delta = -2.9$ mW/cm^2. The absence of such a maximum in the data is troubling and will require further investigation. Data were obtained for I as low as 5 mW/cm^2 for $\Delta = -2.3\Gamma$, and 4.3 mW/cm^2 for $\Delta = -2.9\Gamma$. At smaller I, the atomic fluorescence is too weak to acquire reliable data.

The Δ dependence of B_{FS} is significant and is striking in its disagreement with present theory. B_{FS} is found to decrease by a factor of 6 as Δ is changed from -2.3Γ to -3.5Γ, while JWDB predict a far smaller, ~60%, decrease. With their theory, which neglects hyperfine effects, JWDB find that B_{FS} depends weakly on Δ for $|\Delta| > 2\Gamma$ but that B_{FS} should increase rapidly for $|\Delta| < 2\Gamma$ due to contributions from the 2_u state. They discuss the possibility that the relative contributions from the 0_u^+ and 2_u states may be altered when hyperfine interactions are accounted for [11]. In light of the present disagreement, we look forward to the incorporation of hyperfine effects into the theory.

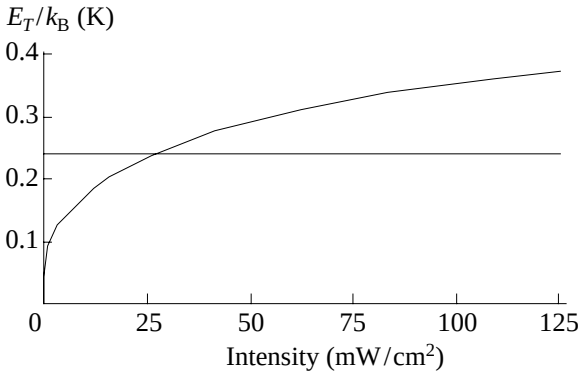

Fig. 5. Calculated trap depth in the shallowest direction (z-axis) of our six-beam MOT as a function of total trap laser intensity for $\Delta = -3.5\Gamma$. The horizontal line indicates the depth 1/2 ΔE_{FS}.

A comparison between experiment and theory for the RE process provides a sensitive test of the validity of the theory for this process and reinforces the importance of accurate knowledge of trap depth [9]. It has been predicted that RE rates for Li depend much more strongly on E_T than for other alkali species because decay from attractive molecular states leading to RE is symmetry forbidden, in the Hund's case (a) region, where the molecular interaction exceeds the relatively weak fine-structure interaction [25]. In the Hund's case (a) region, the RE loss rates have been predicted to scale as $E_T^{-17/6}$ [25]. We have fit the actual RE rates calculated by JWDB for various values of E_T to a power law, E_T^{-a}, for each of the four detunings. For each of the detunings, the best fit is for $a = 3.04$, close to the predicted value of 17/6. Since E_T depends strongly on both I and Δ, a useful comparison between experiment and theory requires accurate knowledge of E_T, including trap depth anisotropy. Therefore, the calculated RE loss rates shown in Fig. 2 as solid lines are averaged over all directions as

$$\beta = \frac{\beta_0}{4\pi}\int\left(\frac{E_T(\theta,\phi)}{E_0}\right)^{-a} d\Omega, \quad (9)$$

where β_0 is calculated for a symmetric trap of depth E_0. We find, for E_0 equal to the trap depth in the shallowest direction, $\beta/\beta_0 = 0.22 \pm 0.02$ and is relatively independent of I and Δ. The calculated results shown in Fig. 2 assume that the temperature of the trapped atoms is 1 mK, based on the result of a single measurement using the time-of-flight technique [26]. JWDB predict the loss rate to be relatively insensitive to temperature in the range 0.3 to 3 mK, the rate at 0.3 mK being approximately 60% of the rate at 3 mK [11].

Without the effect of E_T, RE loss rates should rise with intensity as the excited-state fraction increases. However, when E_T is accounted for, the calculated loss rates are nearly independent of I. Theoretically, the increase in loss rate due to a larger excited-state fraction is compensated by an increase in trap depth. The comparison between experiment and theory depicted in Fig. 2 is good at low intensities near the fine-structure turn-off, where the minimum trap depth is known unambiguously. However, at higher intensities, the measured loss rates clearly increase with I, at odds with JWDB's calculations using our calculated values of E_T. As an example of the calculated intensity dependence of E_T, Fig. 5 shows E_T in the shallowest direction (along the z-axis) versus I for $\Delta = -3.5\Gamma$.

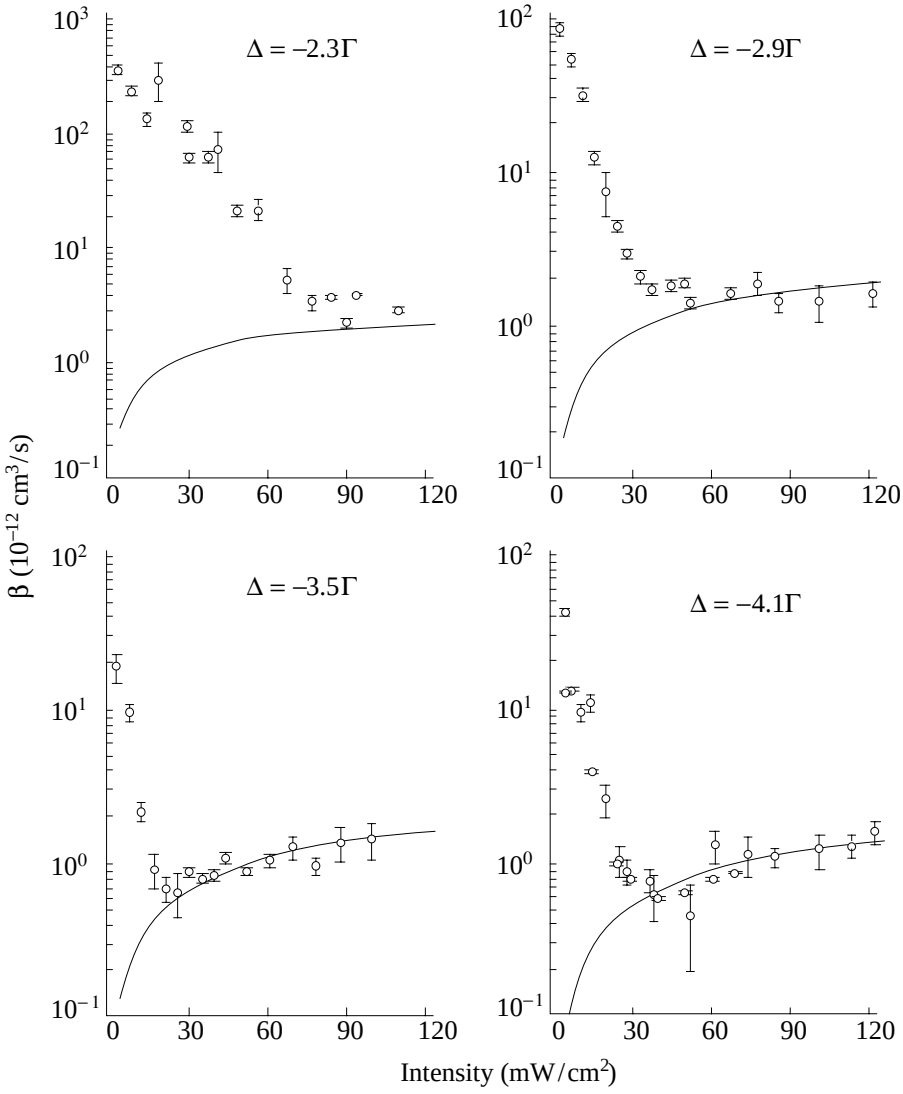

Fig. 6. Comparison of measured RE rates (open circles) with the function 10^{-11} cm^3/s $\rho_e(1-\rho_e)$ (solid lines). This function assumes that the RE rates have no trap depth dependence.

Figure 6 shows an alternative comparison with the data, where the effects of trap depth are neglected. The solid lines represent the function 10^{-11} cm^3/s $\rho_e(1-\rho_e)$, where ρ_e is the excited-state fraction calculated using equation (2) and is a function of both I and Δ. This model is consistent with the Gallagher–Pritchard model [1], where the calculated loss rates vary by less than a factor of 2 in the relevant range of detunings. In addition, the radiative escape probability in the Gallagher–Pritchard model is relatively insensitive to trap depth since the time the atoms spend in the region of small interatomic separation R, where RE decay occurs, is small compared to the radiative lifetime, and the radiative decay rates are assumed to be independent of R. JWDB's more sophisticated calculation accounts for the variation of the radiative coupling strength with R, leading to the strong E_T^{-3} trap depth dependence for Li. However, assuming the trap depth model is correct, the intensity dependence of our data is more consistent with the simpler model. The results of Kawanaka *et al.*, who use a different technique to vary trap depth, are consistent, the RE loss rate being independent of trap depth [8]. In their case, the trap depth was actually measured [22].

There is also a discrepancy between the observed and calculated detuning dependence of the RE rates. The observed loss rate coefficients are found to be relatively insensitive to Δ, whereas the predicted rates are approximately seven times smaller for $\Delta = -4.1\Gamma$ than for $\Delta = -2.3\Gamma$ at $I = 120$ mW/cm^2. In Fig. 7, the trap depth corresponding to the shallowest direction (z-axis) is plotted versus Δ for $I = 120$ mW/cm^2. From $\Delta = -2.3\Gamma$ to -4.1Γ, E_T increases by a factor of 1.7, which should suppress the RE loss rate by a factor of 5, relative to the case where trap depth does not depend on detuning. Therefore, most of the discrepancy is accounted for by

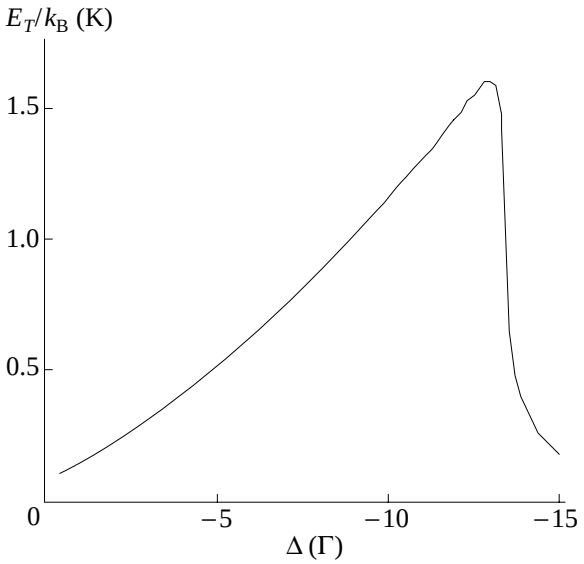

Fig. 7. Calculated trap depth in the shallowest direction (z-axis) of our six-beam MOT as a function of Δ for $I = 120$ mW/cm^2. The trap depth at the larger detunings is only illustrative of the model predictions and is not expected to be accurate since the spring-constant of the trap is insufficient to contain atoms to dimensions small compared to the trap laser beam size.

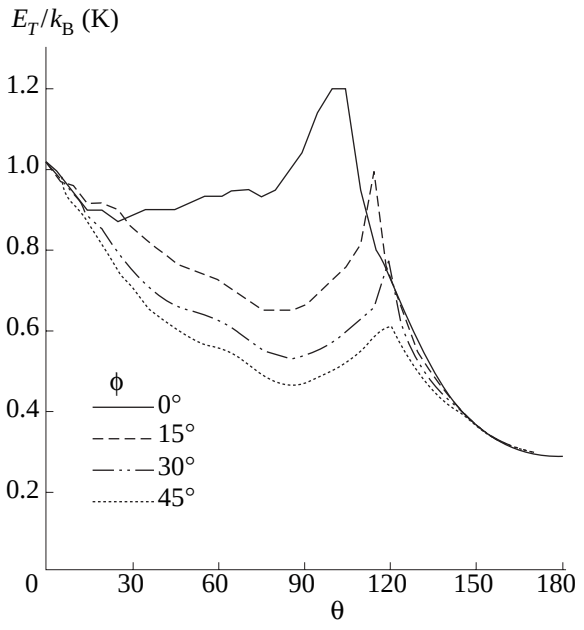

Fig. 8. Angular variation of trap depth for the four-beam tetrahedral MOT described in [8] with $\Delta = -22$ MHz. The total intensity in the four beams is 30 mW/cm^2 for the frequency tuned near the resonance frequency of $F = 2$ ground-state atoms and 10 mW/cm^2 for the frequency tuned near the resonance frequency of $F = 1$ ground-state atoms. The horizontal axis corresponds to the polar angle relative to the trap beam that is along the symmetry axis of the field coils. The trap depth is shown for four azimuthal angles that span one-sixth of a sphere, which, by symmetry, gives E_T for the complete surface area of the tetrahedral MOT. The field gradient is 34 G/cm along the symmetry axis, and the laser polarizations are circular, as defined in [8].

trap depth. This discrepancy might again be a manifestation of the neglect of hyperfine structure in the calculations or may indicate a breakdown of the E_T model at larger detunings. The origin of these differences is not yet understood. The large detuning range shown in Fig. 7 is only meant to illustrate the trap depth model; the model is expected to be inaccurate at the largest detunings where a weaker trap spring constant invalidates the assumption that atoms are released from the trap center. As can be seen in Fig. 2, the intensity for which FS loss is suppressed at the largest detuning is less accurately predicted by the trap depth calculation. The dimensions of the trapped atom cloud are observed to increase for larger Δ, and the spring constant is found to be insufficient to trap atoms for the largest detunings shown in Fig. 7.

Finally, we calculate the trap depth for the ^{7}Li collisional trap loss experiment of Kawanaka *et al.* [8]. Their experimental setup differs in several respects from ours: (1) they employ a tetrahedral four-beam MOT; (2) the intensities of the two trap laser frequencies are not equal; and (3) they rapidly modulate (500 kHz) the trap beams on and off, so that E_T may be varied via the chop duty cycle. They observe the suppression of FS for a duty cycle of 70% and $\Delta = -8$ MHz [8]. Our trap depth model for this trap with a 100% duty cycle predicts that $E_T/k_B = 81$ mK in the shallowest direction, which is too low to suppress FS. However, if $\Delta = -22$ MHz instead, and if 70% duty cycle is assumed to be equivalent to a continuous intensity of 70% of the maximum value, we find good agreement with their observed trap depth. (The authors of [8] now believe that the detuning in their experiment may have been greater in magnitude than 8 MHz but not as great as 22 MHz [21].) Figure 8 shows the calculated angular dependence of trap depth of a four-beam MOT for $\Delta = -22$ MHz. In the sextant of the sphere shown, the trap lasers propagate through the trap center along the (0, 0) and (109.5°, 0°) directions. An atom sees the deepest trap potential when its velocity copropagates with a trap laser beam. As in the model of the six-beam MOT, the shallowest directions correspond to an atom counterpropagating with a trap beam. The prediction that $E_T(0, 0)/E_T(90°, 30°) = 2$ agrees with experiment [22]. In the four-beam MOT, an atom can actually be accelerated out of the trap by three of the beams when its initial velocity is greater than $|3\Delta/k|$ and directed into the fourth beam. Using the theory of JWDB and equation (9) for the effective trap depth gives a value for β of 4.3×10^{-13} cm^3/s at a 100% duty cycle, for $\Delta = -22$ MHz, which agrees well with their measured value of 4.5×10^{-13} cm^3/s (although at their measured Δ of −8 MHz). As mentioned previously, in the low-intensity regime, Kawanaka *et al.* observe the RE rate to increase linearly with duty cycle [8], and they also measure the trap depth to increase linearly with duty cycle [22]. Therefore, both experiments are consistent with weak trap depth dependence in the rate of RE.

Recent work by Peters *et al.* in Rb using an independent catalysis laser tuned red of the $P_{1/2}$ level also reports the observation of RE without FS [27].

5. CONCLUSION

We have presented a three-dimensional model of trap depth that includes all relevant atomic levels and applied this model to the analysis of radiative escape and fine-structure changing trap loss collisions in ^{7}Li. The ability to suppress FS as a trap loss mechanism enables the separation of the contributions of RE and FS. When trap depth is taken into account, the semiclassical optical Bloch theory of [11] agrees well with the measured RE rates at intensities and detunings where the trap depth is known unambiguously by the turnoff of FS as a loss mechanism. However, both the detuning and intensity dependence of the FS and the RE rates are inconsistent with current theory when trap depth is either calculated (our experiment) or measured (experiment of Kawanaka *et al.*). In particular, the strong E_T^{-3} trap depth dependence predicted by theory for RE is not observed. The origin of the discrepancies is not yet understood and remains a challenge for future experimental and theoretical work. In the future, we plan to extend our work to ^{6}Li to investigate the role that hyperfine interactions may play in resolving these discrepancies.

Finally, our investigations point out the necessity of accurate knowledge of trap depth in order to make realistic comparisons between experiment and theory. The depth of a MOT is a complicated function of all the parameters of the trap, including trap laser detuning, intensity, beam size, and magnetic field gradient, which must be carefully measured or calculated for every experimental setup.

ACKNOWLEDGMENTS

This work was supported by the National Science Foundation, the Texas Advanced Technology Program, and the Robert A. Welch Foundation. We gratefully acknowledge productive interactions with P.S. Julienne and the valuable contributions to the experiment made by B.P. Anderson, C.C. Bradley, and Y.Y. Xiao.

REFERENCES

1. Vigué, J., 1986, *Phys. Rev. A*, **34**, 4476; Julienne, P.S., Pan, S.H., Thorsheim, H.R., *et al.*, 1988, *Advances in Laser Science*, Tam, A.C., Gole, J.L., and Stwalley, W.C., Eds. (New York: AIP), vol. **3**, p. 308; Gallagher, A. and Pritchard, D.E., 1989, *Phys. Rev. Lett*., **63**, 957.
2. Prentiss, M., Cable, A., Bjorkholm, J.E., *et al.*, 1988, *Opt. Lett.*, **13**, 452.
3. Marcassa, L., Bagnato, V., Wang, Y., *et al.*, 1993, *Phys. Rev. A*, **47**, R4563.
4. Sesko, D., Walker, T., Monroe, C., *et al.*, 1989, *Phys. Rev. Lett.*, **63**, 961.
5. Hoffmann, D., Feng, P., Williamson, R.S. III, *et al.*, 1992, *Phys. Rev. Lett*., **69**, 753.
6. Wallace, C.D., Dinneen, T.P., Tan, K.-Y.N., *et al.*, 1992, *Phys. Rev. Lett*., **69**, 897.
7. Feng, P., Hoffmann, D., and Walker, T., 1993, *Phys. Rev. A*, **47**, R3495.
8. Kawanaka, J., Shimizu, K., Takuma, H., *et al.*, 1993, *Phys. Rev. A*, **48**, R883.
9. Ritchie, N.W.M., Abraham, E.R.I., Xiao, Y.Y., *et al.*, Submitted for publication.
10. Lindquist, K., Stephens, M., and Wieman, C., 1992, *Phys. Rev. A*, **46**, 4082.
11. Julienne, P.S., Williams, C., Dulieu, O., *et al.*, 1994, *Laser Physics* (in press).
12. Schmidt-Mink, I., Müller, W., and Meyer, W., 1985, *Chem. Phys.*, **92**, 263.
13. Raab, E.L., Prentiss, M., Cable, A., *et al.*, 1987, *Phys. Rev. Lett.*, **59**, 2631.
14. Wineland, D.J. and Itano, W.M., 1979, *Phys. Rev. A*, **20**, 1521; Stenholm, S., 1986, *Rev. Mod. Phys*., **58**, 699.
15. Bergeman, T., Erez, G., and Metcalf, H., 1987, *Phys. Rev. A*, **35**, 1535.
16. Sobelman, I.I., 1992, *Atomic Spectra and Radiative Transitions* (Berlin: Springer), 2nd ed.
17. Bradley, C.C., Story, J.G., Tollett, J.J., *et al.*, 1992, *Opt. Lett*., **17**, 349.
18. Walker, T., Sesko, D., and Wieman, C., 1990, *Phys. Rev. Lett*., **64**, 408.
19. Sesko, D.W., Walker, T.G., and Wieman, C.E., 1991, *J. Opt. Soc. Am. B*, **8**, 946.
20. Steane, A.M., Chowdhury, M., and Foot, C.J., 1992, *J. Opt. Soc. Am. B*, **9**, 2142.
21. Shimizu, F., 1994, personal communication.
22. Kawanaka, J., Shimizu, K., and Takuma, H., 1993, *Appl. Phys. B*, **57**, 113.
23. Monroe, C., Swann, W., Robinson, H., *et al.*, 1990, *Phys. Rev. Lett.*, **65**, 1571.
24. Band, Y.B. and Julienne, P.S., 1992, *Phys. Rev. A*, **46**, 330.
25. Julienne, P.S. and Vigué, J., 1991, *Phys. Rev. A*, **44**, 4464.
26. Lett, P.D., Watts, R.N., Westbrook, C.I., *et al.*, 1988, *Phys. Rev. Lett.*, **61**, 169.
27. Peters, M.G., Hoffmann, D., Tobiason, J.D., *et al.*, Submitted for publication.